Multiqubit tunable phase gate of one qubit simultaneously controlling *n* qubits in a cavity

Chui-Ping Yang,[1,2,3,5] Shi-Biao Zheng,[1,4] and Franco Nori[1,2]
[1]*Advanced Science Institute, RIKEN, Wako-Shi, Saitama 351-0198, Japan*
[2]*Physics Department, The University of Michigan, Ann Arbor, Michigan 48109-1040, USA*
[3]*Department of Physics, Hangzhou Normal University, Hangzhou, Zhejiang 310036, China*
[4]*Department of Physics and State Key Laboratory Breeding Base of Photocatalysis, Fuzhou University, Fuzhou 350002, China*
[5]*State Key Laboratory of Precision Spectroscopy, Department of Physics, East China Normal University, Shanghai 200062, China*
(Received 9 August 2010; revised manuscript received 8 November 2010; published 27 December 2010)

We propose how to realize a multiqubit tunable phase gate of one qubit simultaneously controlling *n* qubits with four-level quantum systems in a cavity or coupled to a resonator. Each of the *n* two-qubit controlled-phase (CP) gates involved in this multiqubit phase gate has a shared control qubit but a *different* target qubit. In this proposal, the two lowest levels of each system represent the two logical states of a qubit while the two higher-energy intermediate levels are used for the gate implementation. The method presented here operates essentially by creating a single photon through the control qubit, which then induces a phase shift to the state of each target qubit. The phase shifts on each target qubit can be adjusted by changing the Rabi frequencies of the pulses applied to the target qubit systems. The operation time for the gate implementation is independent of the number of qubits, and neither adjustment of the qubit level spacings nor adjustment of the cavity mode frequency during the gate operation is required by this proposal. It is also noted that this approach can be applied to implement certain types of significant multiqubit phase gates (e.g., the multiqubit phase gate consisting of *n* two-qubit CP gates which are key elements in quantum Fourier transforms). A possible physical implementation of our approach is presented. Our proposal is quite general and can be applied to physical systems such as various types of superconducting devices coupled to a resonator and trapped atoms in a cavity.

DOI: 10.1103/PhysRevA.82.062326 PACS number(s): 03.67.Lx, 42.50.Dv

I. INTRODUCTION

During the past decade various physical systems have been considered for building up quantum information processors [1–4]. Among them, cavity QED analogs with solid-state systems are particularly appealing [5–10]. Theoretically, it was predicted that the strong-coupling limit, which is difficult to achieve with atoms in a microwave cavity, can be readily realized with superconducting charge qubits [11–13], superconducting flux qubits [14], or semiconducting quantum dots [15]. Moreover, the strong coupling cavity QED has been experimentally demonstrated with superconducting qubits [16,17] and semiconductor quantum dots embedded in a microcavity [18]. These experimental results make solid-state qubit cavity QED a very attractive approach to quantum information processing. The goal of this work is to try to find ways to implement multiqubit gates in solid-state QED qubit systems. Let us first introduce two-qubit gates and then generalize to multiqubit gates.

A. Two-qubit controlled phase gates

It has been shown that standard two-qubit controlled-phase (CP) gates, together with single-qubit gates, form the building blocks of quantum information processors. A standard two-qubit CP gate is described by the transformation $|00\rangle \rightarrow |00\rangle, |01\rangle \rightarrow |01\rangle, |10\rangle \rightarrow |10\rangle$, and $|11\rangle \rightarrow -|11\rangle$. This shows that when the control qubit (the first qubit) is in the state $|1\rangle$, the gate flips the phase of the state $|1\rangle$ of the target qubit (the second qubit) by π (i.e., $|1\rangle \rightarrow -|1\rangle$), but does nothing otherwise. So far, a large number of theoretical proposals for realizing this two-qubit CP gate have been presented with many physical systems. Moreover, this two-qubit CP gate, together with a two-qubit controlled-not (CNOT) gate or a two-qubit *i*SWAP gate, has been experimentally demonstrated in cavity QED [19,20], NMR [21], and superconducting qubits [22–25].

In this paper, we focus on a different type of two-qubit CP gate. To see the difference between this type of gate and the previously mentioned standard CP gate, let us first consider a two-qubit CP gate with qubit 1 (the control qubit) and qubit k (the target qubit). Here, k is the label of the target qubit, which is an integer greater than 1. The operator describing this gate is given by the following matrix

$$R_{1k}(\theta_k) = \begin{pmatrix} 1 & 0 & 0 & 0 \\ 0 & 1 & 0 & 0 \\ 0 & 0 & 1 & 0 \\ 0 & 0 & 0 & e^{i\theta_k} \end{pmatrix}, \tag{1}$$

where $0 \leqslant \theta_k \leqslant 2\pi$. Namely, if and only if the control qubit 1 is in the state $|1\rangle$, a phase shift $e^{i\theta_k}$ happens to the state $|1\rangle$ of the target qubit k. It is obvious that for $\theta_k \neq \pi$, this two-qubit *tunable* CP gate of Eq. (1) is different from the standard two-qubit CP gate. It is called tunable because θ_k can be adjusted, as described in the following.

B. Multiqubit phase gates

Let us now consider a multiqubit quantum phase gate which consists of *n* two-qubit CP gates as depicted in Fig. 1. From Fig. 1, one can see that the *n* two-qubit CP gates act on different qubit pairs (1,2), (1,3), ..., and $(1,n+1)$, respectively. Each two-qubit CP gate has a common control qubit (qubit 1) but a *different* target qubit (2,3, ..., or $n+1$). The CP gate acting on the qubit pair $(1,k)$ is described by the previous operator

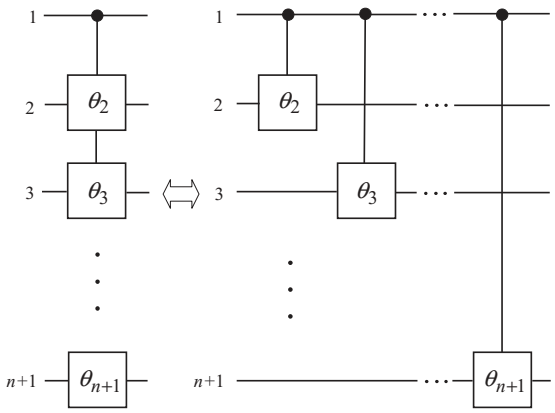

FIG. 1. Schematic circuit of a multiqubit CP gate with one qubit (on top) *simultaneously* controlling n target qubits. The circuit on the left side is equivalent to the circuit on the right side. Each of the n two-qubit CP gates forming this multiqubit phase gate has a shared control qubit (i.e., qubit 1, represented by the filled circle located on top), but a different target qubit (i.e., either qubit $2,3,\ldots,$ or $n+1$). The element θ_k represents a CP shift by $e^{i\theta_k}$, which is performed on the target qubit k when the control qubit 1 is in the state $|1\rangle$ ($k=2,3,\ldots,n+1$). Namely, if the control qubit 1 is in the state $|1\rangle$, then a phase shift $e^{i\theta_k}$ happens to the state $|1\rangle$ of the target qubit k; otherwise nothing happens.

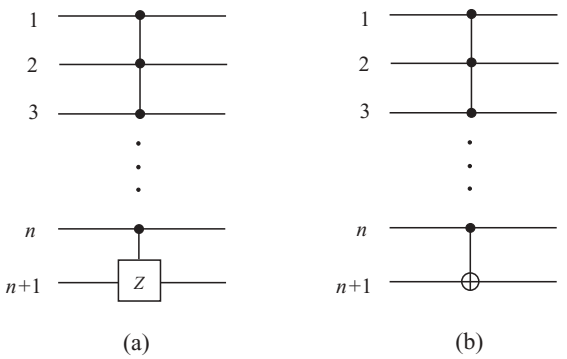

FIG. 2. (a) Schematic circuit of a multiqubit CP gate with n control qubits acting on one target qubit located at the bottom of the circuit shown here. The element Z represents a Pauli rotation σ_z, that is, a phase shift by π around the z axis (with n control qubits on the filled circles). Namely, if the n control qubits are *all* in the state $|1\rangle$, then the state $|1\rangle$ at Z is phase shifted by π (i.e., $|1\rangle \rightarrow e^{i\pi}|1\rangle = -|1\rangle$); otherwise nothing happens to the state at Z. (b) Schematic circuit of a multiqubit controlled-NOT gate with n control qubits acting on one target qubit. The symbol $\oplus$ represents a controlled-NOT gate (with n control qubits on the filled circles). If the n control qubits are *all* in the state $|1\rangle$, then the state at $\oplus$ is bit-flipped (i.e., $|1\rangle \rightarrow |0\rangle$ and $|0\rangle \rightarrow |1\rangle$).

R_{1k}, which induces a phase shift $e^{i\theta_k}$ to the state $|1\rangle$ of the target qubit k when the control qubit 1 is in the state $|1\rangle$. In the general case, any two of the phase shifts $e^{i\theta_2}, e^{i\theta_3}, \ldots, e^{i\theta_{n+1}}$ for the n two-qubit CP gates can be the same or different, and any one of them can be arbitrary. The operator characterizing this multiqubit phase gate with one qubit simultaneously controlling the n target qubits is

$$U = \otimes_{k=2}^{n+1} R_{1k}, \tag{2}$$

where the operator R_{1k} is given by Eq. (1).

C. Motivation for studying multiqubit gates

There are several motivations for this work:

(i) Quantum gates with multiple control qubits or multiple target qubits are of great importance in quantum information processing such as realizing quantum error-correction protocols, constructing quantum circuits, and implementing quantum algorithms. When using the conventional gate-decomposition protocols to construct a multiqubit controlled gate [26,27], the procedure usually becomes complicated (especially for a large n), as the number of single-qubit and two-qubit gates required for the gate implementation heavily depends on the number n of qubits, and therefore building a multiqubit gate may become very difficult.

(ii) Recently, attention is shifting to the physical realization of multiqubit gates (e.g. [28]). Although several methods for implementing multiqubit gates based on cavity QED or trapped ions have been proposed [29–32], realization of *controllable* multiqubit phase gates based on cavity QED or ion traps has not been thoroughly investigated.

(iii) The methods previously proposed [29–32] are mainly for realizing quantum CP or controlled-not gates with *multiple-control* qubits acting on *one target* qubit (Fig. 2). These methods provide a simple and/or fast way for realizing quantum gates with multiple control qubits (a type of multiqubit gate significant in quantum information processing), when compared with the conventional gate-decomposition approaches. However, it is noted that these proposals cannot be extended to perform a different kind of important multiqubit phase gate (i.e., quantum phase gates with one qubit simultaneously controlling multiple target qubits).

D. Advantages

The purpose of this work is to find a way of implementing a multiqubit *tunable* phase gate of one qubit simultaneously controlling n qubits with four-level quantum systems in a cavity or coupled to a resonator. Our proposal operates essentially by creating a single photon through the control qubit, which then induces a phase shift to the state of each target qubit. As shown in the following, this proposal has the following advantages:

(i) Since the excited level $|3\rangle$ is unpopulated during the gate operation, decoherence due to spontaneous decay from this level is suppressed;

(ii) Neither adjustment of the level spacings of qubit systems nor adjustment of the cavity mode frequency during the gate operation is needed, thus the operation is much simplified;

(iii) The operation time required for the gate realization is independent of the number of qubits and thus does not increase with the number of qubits;

(iv) The phase shift on each target qubit can be adjusted by varying the Rabi frequencies of the microwave pulses applied to the target qubit systems; and

(v) The n two-qubit CP gates forming this multiqubit phase gate can be simultaneously performed using six operational

steps (independent of n). Thus, the gate operation is much simplified, especially when the number n is large. In addition, as shown in the following, the present method can be applied for implementing certain types of significant multiqubit phase gates (e.g., the multiqubit phase gate consisting of n two-qubit successive CP gates) which are key elements in the quantum Fourier transform (QFT).

We stress that this proposal is quite general, and can be applied to physical systems such as trapped atoms in a cavity and various types of superconducting qubit systems coupled to a resonator. We note that implementing a *two-qubit* tunable phase gate with two atoms based on cavity QED was previously proposed [33,34]. However, to the best of our knowledge, no one has yet demonstrated how to perform a *multiqubit* tunable phase gate with one qubit simultaneously controlling n qubits in cavity QED. Also, our work shows how to perform the n successive two-qubit CP gates in QFT by the use of only *one* single-mode cavity. We believe that this proposal is useful since it provides a simple and general protocol for realizing a multiqubit phase gate for which the phase shift on each target qubit is *tunable*.

This paper is organized as follows. In Sec. II, we briefly review the basic theory of four-level quantum systems coupled to a single-mode cavity and/or driven by classical pulses. In Sec. III, we show how to realize a multiqubit tunable phase gate with one qubit simultaneously controlling n target qubits, by the use of $(n+1)$ qubit systems in a cavity. In Sec. IV, we discuss how to apply the present method for implementing two types of significant quantum phase gates with multiple target qubits or multiple control qubits. In Sec. V, we give a brief discussion of the experimental feasibility for implementing a six-qubit CP gate, which are key elements in producing a QFT. In Sec. VI, we compare our work with previous work. A concluding summary is presented in Sec. VII.

II. SYSTEMS INTERACTING WITH A CAVITY AND PULSES

The four-level quantum systems throughout this paper could be either natural atoms or *artificial* atoms (e.g., superconducting devices), which have the four levels shown in Fig. 3. Note that the four-level structure in Fig. 3(a) applies to superconducting charge-qubit systems [1], the one in Fig. 3(b) applies to phase-qubit systems [2,35], and the one in Fig. 3(c) applies to flux-qubit systems [1,36]. In addition, the four-level structure in Fig. 3(b) is also available in atoms. By adjusting the level spacings of the qubit systems or the cavity mode frequency, the level $|0\rangle$ can be made not to be affected by the cavity mode or the classical pulses (see the discussion given in the Appendix). Under this condition, the level $|0\rangle$ can be dropped from the discussion in the following (also, see Fig. 4). We note that four levels are needed. This is because (as explained in Sec. III) a three-level quantum system is not enough to implement our desired gate.

A. System-cavity-pulse resonant Raman coupling

Let us consider a qubit system in a cavity or coupled to a resonator, which has a four-level structure depicted in Fig. 3. The energy eigenvalues for the three levels $|1\rangle$, $|2\rangle$, and $|3\rangle$ are denoted as E_1, E_2, and E_3, respectively. Assume that the cavity mode is coupled to the $|2\rangle \leftrightarrow |3\rangle$ transition, but decoupled (highly detuned) from the transition between any other two levels [Fig. 4(a)], which can be achieved by (i) changing the cavity mode frequency, (ii) choosing the qubit system (e.g., atom) appropriately to have a desired level structure, and/or (iii) adjusting the level spacings of the qubit system. Note that the cavity mode frequency for both optical cavities and microwave cavities can be changed in various experiments (e.g., see [37–41]). And, for superconducting qubit systems, the level spacings can be readily adjusted by varying the external parameters (e.g., the external magnetic flux and gate voltage for superconducting charge-qubit systems, the current bias or flux bias in the case of superconducting phase-qubit systems and flux-qubit systems, see, e.g. [1,2]). In addition, we assume that a classical pulse is applied to the qubit system, which is coupled to the $|1\rangle \leftrightarrow |3\rangle$ transition but decoupled (highly detuned) from the transition between any other two levels [Fig. 4(a)]. The Hamiltonian of the whole system can thus be written as

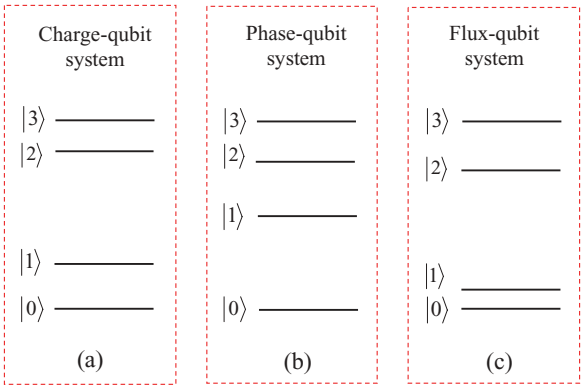

FIG. 3. (Color online) Illustration of four-level qubit systems. The energy eigenvalues for the four levels $|0\rangle$, $|1\rangle$, $|2\rangle$, and $|3\rangle$ are denoted by E_0, E_1, E_2, and E_3, respectively. In (a), the level spacings satisfy $E_2 - E_1 > E_1 - E_0, E_3 - E_2$ and $E_3 - E_2 < E_1 - E_0$. In (b), the level spacings satisfy $E_1 - E_0 > E_2 - E_1 > E_3 - E_2$. In (c), the level spacings meet $E_2 - E_1 > E_1 - E_0, E_3 - E_2$ and $E_3 - E_2 > E_1 - E_0$. The four-level structure in (a) applies to charge-qubit systems, the one in (b) applies to phase-qubit systems, and the one in (c) applies to flux-qubit systems. In addition, the four-level structure in (b) is also available in atoms.

$$H = \hbar\omega_c a^\dagger a + \sum_{l=1}^{3} E_l |l\rangle\langle l| + \hbar g(a^\dagger \sigma_{23}^- + \text{H.c.}) + \hbar\Omega(e^{i\omega t}\sigma_{13}^- + \text{H.c.}), \quad (3)$$

where $a^\dagger$ and a are the photon creation and annihilation operators of the cavity mode with frequency ω_c, g is the coupling constant between the cavity mode and the $|2\rangle \leftrightarrow |3\rangle$ transition, Ω is the Rabi frequency of the pulse, and ω is the frequency of the pulse; $\sigma_{23}^- = |2\rangle\langle 3|$ and $\sigma_{13}^- = |1\rangle\langle 3|$.

Let us now assume that the cavity mode is off-resonance with the $|2\rangle \leftrightarrow |3\rangle$ transition (i.e., $\Delta_c = \omega_{32} - \omega_c \gg g$) and the pulse is off-resonance with the $|1\rangle \leftrightarrow |3\rangle$ transition (i.e., $\Delta = \omega_{31} - \omega \gg \Omega$) where $\omega_{32} = (E_3 - E_2)/\hbar$ and $\omega_{31} = (E_3 - E_1)/\hbar$ are, respectively, the $|2\rangle \leftrightarrow |3\rangle$ transition frequency and the $|1\rangle \leftrightarrow |3\rangle$ transition frequency [Fig. 4(a)].

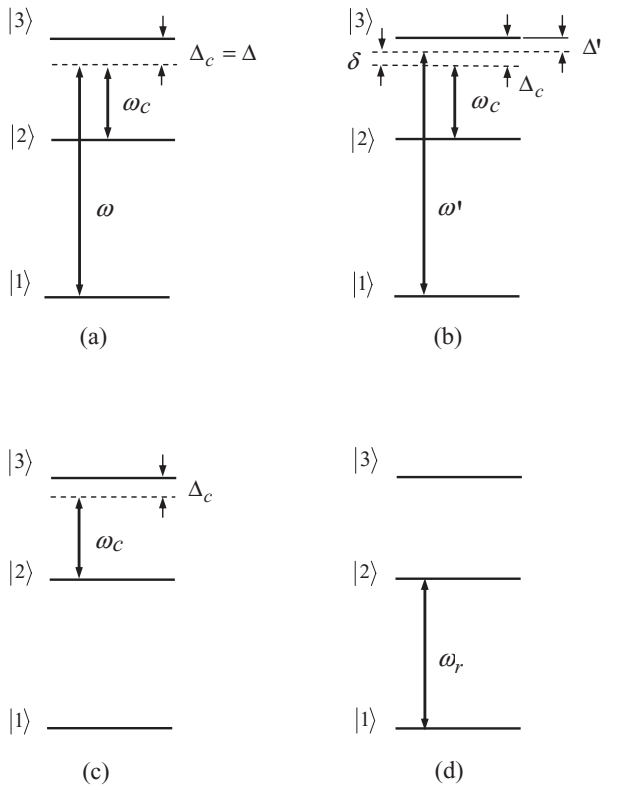

FIG. 4. (a) System-cavity-pulse resonant Raman coupling for a qubit system in a cavity. Here, $\Delta = \omega_{31} - \omega$ is the detuning between the pulse frequency ω and the $|1\rangle \leftrightarrow |3\rangle$ transition frequency ω_{31}, while $\Delta_c = \omega_{32} - \omega_c$ is the detuning between the cavity mode frequency ω_c and the $|2\rangle \leftrightarrow |3\rangle$ transition frequency ω_{32}. The detunings Δ_c and Δ are set to be equal (i.e., $\Delta_c = \Delta$) to establish the resonant Raman coupling between the two levels $|1\rangle$ and $|2\rangle$ of the qubit system. (b) System-cavity-pulse off resonant Raman coupling for n qubit systems $(2,3,\ldots,n+1)$ in a cavity. For simplicity, we here only draw a figure for qubit system k interacting with the cavity mode and a classical microwave pulse $(k = 2,3,\ldots,n+1)$. Here, $\delta = \Delta_c - \Delta'$ is the detuning of the cavity mode with the pulse, $\Delta' = \omega_{31} - \omega'$ is the detuning between the pulse frequency ω' and the $|1\rangle \leftrightarrow |3\rangle$ transition frequency of qubit system k. Note that δ, Δ_c, and Δ' are the same for all qubit systems $(2,3,\ldots,n+1)$ and that the pulses applied to the individual qubit systems $(2,3,\ldots,n+1)$ have the same frequency ω'. The Rabi frequency of the pulse applied to qubit system k is denoted by Ω_k. (c) System-cavity off resonant interaction for n qubit systems $(2,3,\ldots,n+1)$ in a cavity. The cavity mode is off resonant with the $|2\rangle \leftrightarrow |3\rangle$ transition of each qubit system, with a detuning Δ_c. (d) System-pulse resonant interaction. The pulse with a frequency ω_r is resonant with the $|1\rangle \leftrightarrow |2\rangle$ transition.

Under these conditions, the level $|3\rangle$ can be adiabatically eliminated [42]. Thus, for $\Delta_c = \Delta_{\mu w}$, the effective Hamiltonian in the interaction picture is [43]

$$H_I = -\hbar\left[\frac{\Omega^2}{\Delta}|1\rangle\langle 1| + \frac{g^2}{\Delta_c}a^\dagger a|2\rangle\langle 2| + \frac{\Omega g}{\Delta_c}(a^\dagger\sigma_{12}^+ + \text{H.c.})\right] \tag{4}$$

where $\sigma_{12}^+ = |2\rangle\langle 1|$. The first two terms in Eq. (4) are ac-Stark shifts of the levels $|1\rangle$ and $|2\rangle$ induced by the pulse and the cavity mode, respectively; while the last two terms in Eq. (4) are the familiar Jaynes-Cummings interaction, describing the resonant Raman coupling between the two levels $|1\rangle$ and $|2\rangle$, which results from the cooperation of the cavity mode and the pulse.

For the case of $\Omega = g$, the initial states $|2\rangle|1\rangle_c$ and $|1\rangle|0\rangle_c$ of the whole system, under the Hamiltonian (4), evolve as follows:

$$\begin{aligned} |2\rangle|1\rangle_c &\to e^{ig^2t/\Delta_c}[\cos(g^2t/\Delta_c)|2\rangle|1\rangle_c \\ &\quad - i\sin(g^2t/\Delta_c)|1\rangle|0\rangle_c], \\ |1\rangle|0\rangle_c &\to e^{ig^2t/\Delta_c}[-i\sin(g^2t/\Delta_c)|2\rangle|1\rangle_c \\ &\quad + \cos(g^2t/\Delta_c)|1\rangle|0\rangle_c], \end{aligned} \tag{5}$$

where $|0\rangle_c$ and $|1\rangle_c$ are the vacuum state and the single-photon state of the cavity mode, respectively. The state $|0\rangle|0\rangle_c$ remains unchanged under the Hamiltonian (4).

B. System-cavity-pulse off-resonant Raman coupling

Consider n qubit systems labeled by $2,3,\ldots,$ and $n+1$. Each qubit system has a four-level structure, as described previously. The cavity mode is coupled to the $|2\rangle \leftrightarrow |3\rangle$ transition of each qubit system, but decoupled (highly detuned) from the transition between any other two levels [Fig. 4(b)]. In addition, a classical pulse is applied to each one of qubit systems $(2,3,\ldots,n+1)$, which is coupled to the $|1\rangle \leftrightarrow |3\rangle$ transition but decoupled from the transition between any other two levels [Fig. 4(b)]. Each pulse has the same frequency ω'. The Hamiltonian for the whole system in the Schrödinger picture is

$$\begin{aligned} H = {} & \hbar\omega_c a^\dagger a + \sum_{k=2}^{n+1}\Bigg[\sum_{l=1}^{3}E_l|l\rangle_k\langle l| + \hbar g(a^\dagger\sigma_{23,k}^- + \text{H.c.}) \\ & + \hbar\Omega_k(e^{i\omega' t}\sigma_{13,k}^- + \text{H.c.})\Bigg], \end{aligned} \tag{6}$$

where the subscript k represents the kth qubit system, Ω_k is the Rabi frequency of the pulse applied to the kth qubit system, $\sigma_{23,k}^- = |2\rangle_k\langle 3|$, $\sigma_{13,k}^- = |1\rangle_k\langle 3|$, and g is the coupling constant between the cavity mode and the $|2\rangle \leftrightarrow |3\rangle$ transition of each qubit system.

The detuning between the $|1\rangle \leftrightarrow |3\rangle$ transition frequency of the kth qubit system and the frequency of the pulse applied to the kth qubit system is $\Delta' = \omega_{31} - \omega'$ $(k = 2,3,\ldots,n+1)$, which is identical for each qubit system (i.e., independent of k) because of the same frequency ω' of each pulse [Fig. 4(b)]. Under the condition $\Delta_c \gg g$ and $\Delta' \gg \max\{\Omega_2,\Omega_3,\ldots,\Omega_{n+1}\}$, the effective Hamiltonian in the interaction picture can be written as [43]

$$\begin{aligned} H_{\text{eff}} = {} & -\hbar\sum_{k=2}^{n+1}\Bigg[\frac{\Omega_k^2}{\Delta'}|1\rangle_k\langle 1| + \frac{g^2}{\Delta_c}a^\dagger a|2\rangle_k\langle 2| \\ & + \chi_k(e^{-i\delta t}a^\dagger\sigma_{12,k}^+ + \text{H.c.})\Bigg], \end{aligned} \tag{7}$$

where $\sigma_{12,k}^+ = |2\rangle_k\langle 1|$, $\delta = \Delta_c - \Delta'$ and

$$\chi_k = \Omega_k g(1/\Delta_c + 1/\Delta')/2. \tag{8}$$

For $\delta \gg g^2/\Delta_c$, $\delta \gg \max\{\Omega_2^2/\Delta', \Omega_3^2/\Delta', \ldots, \Omega_{n+1}^2/\Delta'\}$, and $\delta \gg \max\{\chi_2, \chi_3, \ldots, \chi_{n+1}\}$, there is no energy exchange between the qubit systems and the cavity mode. Thus, the effective Hamiltonian can be further written as [43–45]

$$\begin{aligned} H_{\text{eff}} = & -\hbar \sum_{k=2}^{n+1} \left(\frac{\Omega_k^2}{\Delta'} |1\rangle_k\langle 1| + \frac{g^2}{\Delta_c} a^\dagger a |2\rangle_k\langle 2| \right) \\ & -\hbar \sum_{k=2}^{n+1} \left[\frac{\chi_k^2}{\delta} (a^\dagger a |2\rangle_k\langle 2| - a a^\dagger |1\rangle_k\langle 1|) \right] \\ & +\hbar \sum_{k\neq k'=2}^{n+1} \frac{\chi_k \chi_{k'}}{\delta} (\sigma_{12,k}^+ \sigma_{12,k'}^- + \sigma_{12,k}^- \sigma_{12,k'}^+), \end{aligned} \tag{9}$$

where the two terms in the second line above describe the photon-number-dependent Stark shifts induced by the off-resonant Raman coupling, and the two terms in the last parentheses describe the "dipole" coupling between the two qubit systems (k,k') mediated by the cavity mode and the classical pulses. In the case when the level $|1\rangle$ of each qubit system is not populated, the Hamiltonian (9) reduces to

$$H_{\text{eff}} = -\hbar \sum_{k=2}^{n+1} \left(\frac{g^2}{\Delta_c} + \frac{\chi_k^2}{\delta} \right) a^\dagger a |2\rangle_k\langle 2|. \tag{10}$$

The time-evolution operator for the Hamiltonian (10) is given by

$$U(t) = \otimes_{k=2}^{n+1} U_{kc}(t), \tag{11}$$

where $U_{kc}(t) = \exp[i(g^2/\Delta_c + \chi_k^2/\delta) a^\dagger a |2\rangle_k\langle 2| t]$ is the time-evolution operator acting on the cavity mode and the kth qubit system, which takes the following form

$$U_{kc}(t) = \begin{pmatrix} 1 & 0 & 0 & 0 \\ 0 & 1 & 0 & 0 \\ 0 & 0 & 1 & 0 \\ 0 & 0 & 0 & e^{i\varphi_k(t)} \end{pmatrix}, \tag{12}$$

in the basis states $|0\rangle_k|0\rangle_c = (1,0,0,0)^T$, $|0\rangle_k|1\rangle_c = (0,1,0,0)^T$, $|2\rangle_k|0\rangle_c = (0,0,1,0)^T$, and $|2\rangle_k|1\rangle_c = (0,0,0,1)^T$. Here $\varphi_k(t) = \exp[i(g^2/\Delta_c + \chi_k^2/\delta)t]$. Note that the conditional phase φ_k is adjustable by varying the Rabi frequency Ω_k [see Eq. (8)].

C. System-cavity off-resonant interaction

Consider n qubit systems $(2,3,\ldots,n+1)$ with the four-level structure described previously. The cavity mode is coupled to the $|2\rangle \leftrightarrow |3\rangle$ transition of each qubit system, but decoupled (highly detuned) from the transition between any other two levels [Fig. 4(c)]. The Hamiltonian for the whole system is given by

$$\begin{aligned} H = & \hbar\omega_c a^\dagger a + \sum_{k=2}^{n+1} \sum_{l=1}^{3} E_l |l\rangle_k\langle l| \\ & +\hbar \sum_{k=2}^{n+1} g\,(a^\dagger \sigma_{23,k}^- + \text{H.c.}), \end{aligned} \tag{13}$$

where the subscript k represents the kth qubit system, $\sigma_{23,k}^- = |2\rangle_k\langle 3|$, and $l = 0,1,2,3$.

In the interaction picture, the Hamiltonian (13) becomes

$$H = \hbar \sum_{k=2}^{n+1} g(e^{-i\Delta_c t} a^\dagger \sigma_{23,k}^- + \text{H.c.}). \tag{14}$$

For the case of $\Delta_c \gg g$ (i.e., the cavity mode is off resonant with the $|2\rangle \leftrightarrow |3\rangle$ transition of each qubit system), no energy exchange occurs between the qubit systems and the cavity mode. Thus, the effective Hamiltonian can be written as [44,45]

$$\begin{aligned} H_{\text{eff}} = & -\hbar \sum_{k=2}^{n+1} \frac{g^2}{\Delta_c} (a^\dagger a \sigma_{22,k} - a a^\dagger \sigma_{33,k}) \\ & +\hbar \sum_{k\neq k'=2}^{n+1} \frac{g^2}{\Delta_c} (\sigma_{23,k}^+ \sigma_{23,k'}^- + \sigma_{23,k}^- \sigma_{23,k'}^+), \end{aligned} \tag{15}$$

where the two terms in the first line above represent the photon-number-dependent Stark shifts, while the two terms in the second line above describe the "dipole" coupling between the two qubit systems (k,k') mediated by the cavity mode. When the level $|3\rangle$ of each qubit system is not excited, the Hamiltonian (15) reduces to

$$H_{\text{eff}} = -\hbar \sum_{k=2}^{n+1} \frac{g^2}{\Delta_c} a^\dagger a \sigma_{22,k}. \tag{16}$$

The time-evolution operator for the Hamiltonian (16) is given by

$$\widetilde{U}(t) = \otimes_{k=2}^{n+1} \widetilde{U}_{kc}(t), \tag{17}$$

where $\widetilde{U}_{kc}(t) = \exp[i(g^2/\Delta_c) a^\dagger a \sigma_{22,k} t]$ is the time-evolution operator acting on the cavity mode and the kth qubit system. The operator $\widetilde{U}_{kc}(t)$ is expressed as

$$\widetilde{U}_{kc}(t) = \begin{pmatrix} 1 & 0 & 0 & 0 \\ 0 & 1 & 0 & 0 \\ 0 & 0 & 1 & 0 \\ 0 & 0 & 0 & e^{i\phi_k(t)} \end{pmatrix}, \tag{18}$$

in the basis states $|0\rangle_k|0\rangle_c = (1,0,0,0)^T$, $|0\rangle_k|1\rangle_c = (0,1,0,0)^T$, $|2\rangle_k|0\rangle_c = (0,0,1,0)^T$, and $|2\rangle_k|1\rangle_c = (0,0,0,1)^T$. Here $\phi_k(t) = \exp(ig^2 t/\Delta_c)$.

D. System-pulse resonant interaction

Consider now a qubit system driven by a classical pulse with frequency ω_r and initial phase ϕ. Moreover, assume that the pulse is resonant with the $|1\rangle \leftrightarrow |2\rangle$ transition (i.e., $\omega_r = \omega_{21}$) where $\omega_{21} = (E_2 - E_1)/\hbar$ is the transition frequency between the two levels $|1\rangle$ and $|2\rangle$ [Fig. 4(d)]. In this case, the interaction Hamiltonian in the interaction picture is given by

$$H_I = \frac{\hbar}{2} (\widetilde{\Omega} e^{i\phi} |1\rangle\langle 2| + \text{H.c.}), \tag{19}$$

where $\widetilde{\Omega}$ is the Rabi frequency of the pulse. From the Hamiltonian (19), it is straightforward to show that a pulse

of duration t results in the following rotation:

$$\begin{aligned} |1\rangle &\to \cos\frac{\widetilde{\Omega}}{2}t|1\rangle - ie^{-i\phi}\sin\frac{\widetilde{\Omega}}{2}t|2\rangle, \\ |2\rangle &\to -ie^{i\phi}\sin\frac{\widetilde{\Omega}}{2}t|1\rangle + \cos\frac{\widetilde{\Omega}}{2}t|2\rangle. \end{aligned} \tag{20}$$

Previously we have introduced four types of interaction of qubit systems with the cavity mode and/or the pulses. The results presented earlier will be employed for the gate implementation discussed in the next section.

III. IMPLEMENTATION OF MULTIQUBIT PHASE GATES

Let us now consider $(n+1)$ identical qubit systems in a single-mode cavity or coupled to a resonator, which are labeled by $1,2,\ldots,$ and $n+1$, respectively. The qubit systems $(1,2,\ldots,n+1)$ each have the four-level configuration depicted in Fig. 3. For each qubit system, the two lowest levels $|0\rangle$ and $|1\rangle$ represent the two logical states of a qubit while the two higher-energy intermediate levels $|2\rangle$ and $|3\rangle$ are used for the gate implementation. In the following, qubit system 1 acts as a *control* while each one of the qubit systems $(2,3,\ldots,n+1)$ plays a *target* role.

To realize the proposed gate, let us assume that the level $|0\rangle$ of each qubit system is not affected by the cavity mode and/or the pulses during the gate operation; and the cavity mode is off-resonance with the $|2\rangle \leftrightarrow |3\rangle$ transition of each qubit system with a detuning Δ_c, but decoupled (highly detuned) from the transition between any other two levels during the entire operation in the following. As mentioned previously, these conditions can be achieved by prior adjustment of the cavity mode frequency [37–41] or the level spacings of the qubit systems before the gate operation [1,2,46], or by appropriately choosing the qubit systems (i.e., atoms) to have the desired level structure. In addition, assume that quantum information is initially stored by the two lowest levels $|0\rangle$ and $|1\rangle$ of each qubit system and the cavity mode is initially in the vacuum state $|0\rangle_c$.

The procedure for realizing the $(n+1)$-qubit phase gate described by Eq. (2) is as follows:

Step (i): Apply a classical pulse to qubit system 1 to induce the Raman transition described in Sec. II A [Fig. 5(a)]. It can be seen from Eq. (5) that after a pulse duration $t_1 = \pi\Delta_c/(2g^2)$, the state $|1\rangle_1|0\rangle_c$ for qubit system 1 and the cavity mode is transformed to the state $|2\rangle_1|1\rangle_c$. Namely, when the qubit system 1 is initially in the state $|1\rangle$, a photon is emitted to the cavity mode after the pulse. On the other hand, the state $|0\rangle_1|0\rangle_c$ remains unchanged during the pulse.

Step (ii): Apply a classical pulse (with $\omega_r = \omega_{21}$ and $\phi = \pi/2$) to qubit system 1 [Fig. 5(b)] and a classical pulse (with $\omega_r = \omega_{21}$ and $\phi = -\pi/2$) to each of the qubit systems $(2,3,\ldots,n+1)$ [Fig. 5(b′)]. The duration of each pulse is set by $t_2 = \pi/(2\widetilde{\Omega})$ (here, $\widetilde{\Omega}$ is the Rabi frequency of each pulse). It can be seen from Eq. (20) that after the pulses, the state $|2\rangle$ of qubit system 1 is transformed to the state $|1\rangle$ while the state $|1\rangle$ of each of qubit systems $(2,3,\ldots,n+1)$ is transformed to the state $|2\rangle$. Note that since both of the two levels $|2\rangle$ and $|3\rangle$ of qubit system 1 are unpopulated after the operation of this step, *the qubit system* 1 *is decoupled from the cavity mode during the operations of steps (iii) and (iv) below* [see Figs. 5(c) and 5(d)].

Step (iii): Apply a classical pulse (with duration t_3) to each of the qubit systems $(2,3,\ldots,n+1)$ to induce the conditional phase shift described in Sec. II B [Fig. 5(c′)]. Since the level $|1\rangle$ for qubit systems $(2,3,\ldots,n+1)$ is not populated after step (ii) above, the effective Hamiltonian of the whole system is given by Eq. (10). Accordingly, the time-evolution operator describing this step is the operator given by Eq. (11) for $t = t_3$, that is,

$$U(t_3) = \otimes_{k=2}^{n+1} U_{kc}(t_3), \tag{21}$$

where $U_{kc}(t_3)$ is the time-evolution operator acting on the cavity mode and qubit system k $(k = 2,3,\ldots,n+1)$, which takes the matrix of Eq. (12) for $t = t_3$.

Step (iv): Wait for a time t_4. Since no pulse is applied to each qubit system and the cavity mode is off-resonance with the $|2\rangle \leftrightarrow |3\rangle$ transition of each of qubit systems $(2,3,\ldots,n+1)$ [Fig. 5(d′)], this is the case discussed in Sec. II C. Note that the level $|3\rangle$ of each qubit system is not excited. Thus, the effective Hamiltonian of the whole system is given by Eq. (16). Consequently, the time-evolution operator describing this step is the operator given by Eq. (17) for $t = t_4$

$$\widetilde{U}(t_4) = \otimes_{k=2}^{n+1} \widetilde{U}_{kc}(t_4), \tag{22}$$

where $\widetilde{U}_{kc}(t_4)$ is the time-evolution operator acting on the cavity mode and qubit system k, taking the matrix of Eq. (18) for $t = t_4$.

Combining Eq. (22) with Eq. (21) leads to

$$\begin{aligned} |2\rangle_k|1\rangle_c \to \exp[ig^2(t_3+t_4)/\Delta_c] \\ \otimes \exp\left[i\chi_k^2 t_3/\delta\right]|2\rangle_k|1\rangle_c. \end{aligned} \tag{23}$$

When $t_3 + t_4 = 2m\pi\Delta_c/g^2$ (m is an integer), the transformation (23) becomes

$$|2\rangle_k|1\rangle_c \to \exp(i\theta_k)|2\rangle_k|1\rangle_c, \tag{24}$$

with

$$\theta_k = \frac{\chi_k^2}{\delta}t_3 = \frac{\Omega_k^2 g^2}{4\delta}\left(\frac{1}{\Delta_c} + \frac{1}{\Delta'}\right)^2 t_3. \tag{25}$$

Note that g, δ, Δ_c, and Δ' are the same for *all* qubit systems $(2,3,\ldots,n+1)$. Therefore, the angle θ_k can be adjusted by changing the Rabi frequency Ω_k of the pulse applied to the qubit system k. The result (24) shows that after the operations of steps (i)–(iv), a phase shift $\exp(i\theta_k)$ happens to the state $|2\rangle$ of the qubit system k, if and only if the cavity mode is in the single-photon state $|1\rangle_c$.

Step (v): Apply a classical pulse (with $\omega_r = \omega_{21}$ and $\phi = -\pi/2$) to qubit system 1 [Fig. 5(e)] and a classical pulse (with

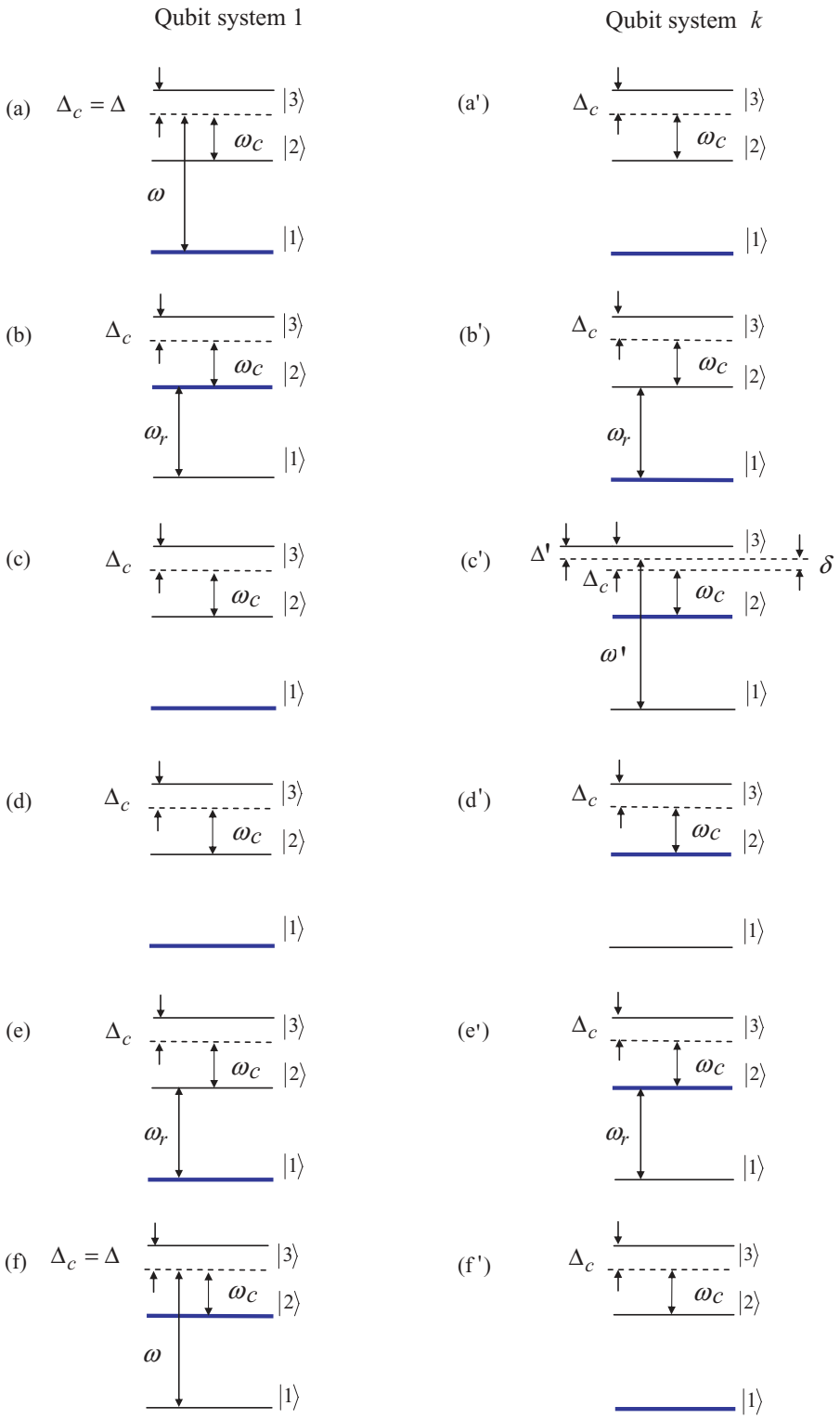

FIG. 5. (Color online) Illustration of qubit systems interacting with the cavity mode and/or the microwave pulses for each step of operations during the gate performance. In each figure, the blue lines represent the level population of qubit systems *before each step of operations*. Figures from top to bottom correspond to the operations of steps (i)–(vi), respectively. The figures on the left side correspond to qubit system 1, while the figures on the right side correspond to qubit system k, with $k = 2,3,\ldots,n+1$. In each figure, $\Delta_c = \omega_{32} - \omega_c$ is the detuning between the cavity mode frequency ω_c and the $|2\rangle \leftrightarrow |3\rangle$ transition frequency ω_{32}. In (a) and (f), $\Delta = \omega_{31} - \omega$ is the detuning between the $|1\rangle \leftrightarrow |3\rangle$ transition frequency ω_{31} and the pulse frequency ω. In (c′), $\Delta' = \omega_{31} - \omega'$ is the detuning between the $|1\rangle \leftrightarrow |3\rangle$ transition frequency ω_{31} and the frequency ω' of the pulse applied to qubit system k, and $\delta = \Delta_c - \Delta'$ is the detuning of the cavity mode with the pulse.

$\omega_r = \omega_{21}$ and $\phi = \pi/2$) to each of qubit systems $(2,3,\ldots,n+1)$ [Fig. 5(e′)]. After a pulse duration $t_2 = \pi/(2\widetilde{\Omega})$, the state $|1\rangle$ of qubit system 1 is transformed to the state $|2\rangle$ while the state $|2\rangle$ of qubit systems $(2,3,\ldots,n+1)$ is transformed back to the original state $|1\rangle$.

Step (vi): Repeat the operation of step (i) [Fig. 5(f)]. After a pulse duration $t_1 = \pi\Delta_c/(2g^2)$, the state $|2\rangle_1|1\rangle_c$ of the qubit system 1 and the cavity mode is changed to the state $|1\rangle_1|0\rangle_c$, which shows that the state $|2\rangle$ of the qubit system 1 is transformed back to the state $|1\rangle$ and the cavity mode returns to its original vacuum state. However, the state $|0\rangle_1|0\rangle_c$ remains unchanged during the pulse.

One can check that the $(n+1)$-qubit phase gate of one qubit simultaneously controlling n qubits, described by Eq. (2), was obtained with $(n+1)$ qubit systems [i.e., the control qubit

system 1 and the target qubit systems $(2,3,\ldots,n+1)$] after the above manipulation.

To better see how the multiqubit phase gate described by Eq. (2) is implemented by the previous operations, let us consider a three-qubit example. One can check that the states of the whole system after each step of the previous operations are summarized below:

$$\begin{aligned}
&|100\rangle|0\rangle_c \quad |200\rangle|1\rangle_c \quad |100\rangle|1\rangle_c\\
&|101\rangle|0\rangle_c \xrightarrow{\text{Step (i)}} |201\rangle|1\rangle_c \xrightarrow{\text{Step (ii)}} |102\rangle|1\rangle_c\\
&|110\rangle|0\rangle_c \quad |210\rangle|1\rangle_c \quad |120\rangle|1\rangle_c\\
&|111\rangle|0\rangle_c \quad |211\rangle|1\rangle_c \quad |122\rangle|1\rangle_c\\
&\xrightarrow{\text{Steps (iii) and (iv)}} \begin{matrix} |100\rangle|1\rangle_c \\ e^{i\theta_3}|102\rangle|1\rangle_c \\ e^{i\theta_2}|120\rangle|1\rangle_c \\ e^{i\theta_2}e^{i\theta_3}|122\rangle|1\rangle_c \end{matrix} \xrightarrow{\text{Step (v)}} \begin{matrix} |200\rangle|1\rangle_c \\ e^{i\theta_3}|201\rangle|1\rangle_c \\ e^{i\theta_2}|210\rangle|1\rangle_c \\ e^{i\theta_2}e^{i\theta_3}|211\rangle|1\rangle_c \end{matrix}\\
&\xrightarrow{\text{Step (vi)}} \begin{matrix} |100\rangle|0\rangle_c \\ e^{i\theta_3}|101\rangle|0\rangle_c \\ e^{i\theta_2}|110\rangle|0\rangle_c \\ e^{i\theta_2}e^{i\theta_3}|111\rangle|0\rangle_c \end{matrix},
\end{aligned} \tag{26}$$

where $|ijk\rangle$ is an abbreviation of the state $|i\rangle_1|j\rangle_2|k\rangle_3$ of qubit systems (1,2,3) with $i,j,k \in \{0,1,2\}$.

On the other hand, it is obvious that the following states of the whole system

$$|000\rangle|0\rangle_c, \quad |001\rangle|0\rangle_c, \quad |010\rangle|0\rangle_c, \quad |011\rangle|0\rangle_c, \tag{27}$$

remain unchanged during the entire operation. Hence, it can be concluded from Eq. (26) that a three-qubit phase gate of one qubit simultaneously controlling two qubits, described by Eq. (2) (with $n=2$), was achieved with three qubit systems (i.e., the control qubit system 1 and the two target qubit systems 2 and 3) after the previous process.

During the operation of step (ii) or (v), a single photon is populated in the cavity mode and the state $|2\rangle$ of each qubit system is occupied. Therefore, for these two-step operations, there is an accumulated phase shift $\exp(i2g^2t_2/\Delta_c)$ to the state $|2\rangle$ of each qubit system. However, when $2t_2 \ll t_3+t_4$, this unwanted phase shift is sufficiently small and thus can be neglected. Note that $t_2=\pi/\widetilde{\Omega}$ and $t_3+t_4=2m\pi\Delta_c/g^2$. Therefore, the condition $2t_2 \ll t_3+t_4$ turns into $\widetilde{\Omega} \gg g^2/(m\Delta_c)$, which can be met by increasing the pulse Rabi frequency $\widetilde{\Omega}$ (i.e., by increasing the intensity of the resonant pulses).

Finally, we should mention that the method proposed here does not work for qubit systems with three levels. Suppose now that the quantum information is encoded in the states $|1\rangle$ and $|2\rangle$. In this case, during the pulse applied to the control qubit system for creating a cavity photon, one cannot have the target qubit systems decoupled from the cavity mode.

IV. TWO TYPES OF MULTIQUBIT PHASE GATES

Previously we have shown how to realize the $(n+1)$-qubit phase gates described by the operator (2). In this section, we focus on two types of multiqubit phase gates, which are depicted in Figs. 6(a) and 7(a), respectively. It can be seen from Figs. 6(a) and 7(a) that the two types of multiqubit phase

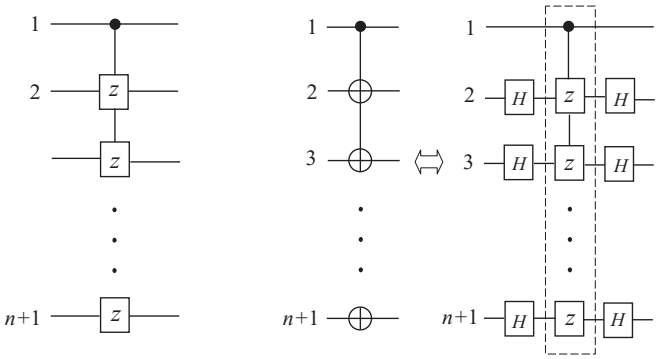

FIG. 6. (a) Circuit for the first type of CP gate with qubit 1 simultaneously controlling n target qubits $(2,3,\ldots,n+1)$. Here, Z represents a CP shift $e^{i\pi}$ on each target qubit. Namely, if the control qubit 1 is in the state $|1\rangle$, then the state $|1\rangle$ at each Z is phase shifted by π (i.e., $|1\rangle \to e^{i\pi}|1\rangle = -|1\rangle$), while the state $|0\rangle$ remains unchanged. (b) Relation between an n-target-qubit controlled-NOT gate and a n-target-qubit CP gate. The circuit on the left side is equivalent to the circuit on the right side. For the circuit on the left side, the symbol $\oplus$ represents a CNOT gate on each target qubit. If the control qubit 1 is in the state $|1\rangle$, then the state at each $\oplus$ is bit flipped as $|1\rangle \to |0\rangle$ and $|0\rangle \to |1\rangle$. However, when the control qubit 1 is in the state $|0\rangle$, the state at each $\oplus$ remains unchanged. On the other hand, for the circuit on the right side, the part enclosed in the dashed-line box represents an n-target-qubit CP gate. The element containing H corresponds to a Hadamard transformation described by $|0\rangle \to (1/\sqrt{2})(|0\rangle+|1\rangle)$ while $|1\rangle \to (1/\sqrt{2})(|0\rangle-|1\rangle)$.

gates considered here consist of n two-qubit CP gates each having a *shared* control qubit but a *different* target qubit. In the following we give a discussion of their implementation and importance in quantum information processing.

A. Implementation of gates of the first type

The CP gate with n-target qubits shown in Fig. 6(a) has the property that the phase for the state $|1\rangle$ of each target qubit is shifted by the same amount π, when the control qubit (i.e., qubit 1) is in the state $|1\rangle$. Hence, this multiqubit phase gate is a special one for $\theta_k=\pi$ and thus the procedure for realizing it is the same as that discussed in the previous section. To obtain this multiqubit phase gate, one needs to set the Rabi frequencies of the pulses applied to the target qubit systems $(2,3,\ldots,n+1)$ to be *identical* (i.e., $\Omega_2=\Omega_3=\cdots=\Omega_{n+1}$, leading to $\chi_2=\chi_3=\cdots=\chi_{n+1}\equiv\chi$) and set the interaction time t_3 to be $t_3=\pi\delta/\chi^2$, such that $\theta_k=\chi_k^2 t_3/\delta=\pi$ $(k=2,3,\ldots,n+1)$.

Note that a controlled-NOT gate with n-target qubits, shown in Fig. 6(b), can also be achieved using the present proposal. This is because this gate is equivalent to the n-target-qubit CP gate discussed here, plus a single-qubit Hadamard gate acting on each target qubit before and after the n-target-qubit CP gate [Fig. 6(b)].

The CP (or controlled-NOT) gates with multiple target qubits shown in Fig. 6(a) [or Fig. 6(b)] are important in quantum information processing because they can be applied in entanglement preparation [47], error correction [48], quantum

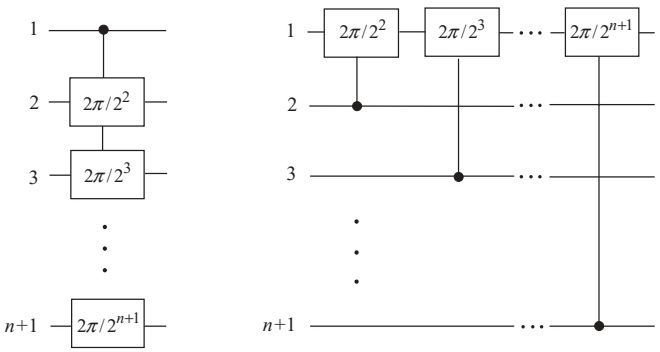

FIG. 7. (a) Circuit for the second type of CP gate with qubit 1 simultaneously controlling n target qubits $(2,3,\ldots,n+1)$. Here, the element $2\pi/2^k$ represents a CP shift $\exp(i2\pi/2^k)$, which is performed on the target qubit k when the control qubit 1 is in the state $|1\rangle$ $(k = 2,3,\ldots,n+1)$. Namely, if the control qubit 1 is in the state $|1\rangle$, then a phase shift $2\pi/2^k$ occurs to the state $|1\rangle$ of the target qubit k, while nothing happens otherwise. (b) Circuit for the n successive two-qubit CP gates in a quantum Fourier transform, which *is equivalent to the circuit in (a).* Here, each two-qubit CP gate has a shared target qubit (i.e., qubit 1) but a different control qubit (i.e., qubit 2, 3, . . . , or, $n+1$). The element $2\pi/2^k$ represents a CP shift $\exp(i2\pi/2^k)$, which is performed on the target qubit 1 when the control qubit k is in the state $|1\rangle$ $(k = 2,3,\ldots,n+1)$. Namely, if the control qubit k is in the state $|1\rangle$, then a phase shift by $2\pi/2^k$ occurs to the state $|1\rangle$ of the target qubit 1, while nothing happens otherwise.

algorithms (e.g., the discrete cosine transform [49]), and quantum cloning [50].

B. Implementation of gates of the second type

The CP gate with n-target qubits shown in Fig. 7(a) has the property that the phase for the state $|1\rangle$ of the target qubit k is shifted by $2\pi/2^k$, when the control qubit (i.e., qubit 1) is in the state $|1\rangle$. Thus, this multiqubit phase gate is a special one for $\theta_k = 2\pi/2^k$ and therefore can be implemented using the procedure introduced in the previous section. To realize it, the Rabi frequencies Ω_2, Ω_3, . . . , and Ω_{n+1} for the pulses (respectively applied to the target qubit systems $2,3,\ldots,$ and $n+1$) need to be set nonidentical, and satisfy the relation $\Omega_{k+1}/\Omega_k = 1/\sqrt{2}$, that is, $\chi_{k+1}/\chi_k = 1/\sqrt{2}$ $(k = 2,3,\ldots,n)$; and the interaction time t_3 above needs to be set by $t_3 = (\pi/2)(\delta/\chi_2^2)$. In this way, we can obtain $\theta_k = \chi_k^2 t_3/\delta = 2\pi/2^k$ $(k = 2,3,\ldots,n+1)$.

For any two-qubit CP gate described by the transformation $|00\rangle \to |00\rangle$, $|01\rangle \to |01\rangle$, $|10\rangle \to |10\rangle$, and $|11\rangle \to e^{i\varphi}|11\rangle$, it is clear that the roles of the two qubits can be interchanged. Namely, the first qubit can be either the control qubit or the target qubit, and the same applies to the second qubit. One can see that when the second (first) qubit is a control qubit, while the first (second) qubit is a target, the phase of the state $|1\rangle$ of the first (second) qubit is shifted by $e^{i\varphi}$ when the second (first) qubit is in the state $|1\rangle$, while nothing happens otherwise. Thus, the quantum circuit in Fig. 7(a) is equivalent to the quantum circuit shown in Fig. 7(b). It can be seen from Fig. 7(b) that each of the n two-qubit CP gates has a shared target qubit (i.e., qubit 1) but a different control qubit (i.e., qubit $2,3,\ldots,$ or $n+1$). Note that the n successive two-qubit CP gates shown in Fig. 7(b) are key elements in QFT [51,52]. Hence, the importance for this second type of multiqubit CP gate is obvious.

The previous discussion shows that the two types of multiqubit CP gates can be implemented by appropriately setting the Rabi frequencies of the pulses applied to the qubit systems. In addition, we should point out that by adjusting the Rabi frequencies of the pulses (i.e., changing the intensities of the pulses) applied to the target qubit systems, other types of quantum CP gates with one qubit simultaneously controlling multiple target qubits, which may have applications in quantum information processing, can, in principle, be performed using this proposal.

V. POSSIBLE EXPERIMENTAL IMPLEMENTATIONS

In this section, we give a discussion on possible experimental implementations. First, as discussed earlier, the condition

$$2t_2 \ll t_3 + t_4,$$

[i.e., $\widetilde{\Omega} \gg g^2/(m\Delta_c)$] needs to be satisfied, which can be achieved by increasing the Rabi frequency $\widetilde{\Omega}$ (i.e., by increasing the intensity of the *resonant pulses*). Second, the total operation time

$$\tau = 2t_1 + 2t_2 + t_3 + t_4 = \pi\Delta_c/g^2 + 2m\pi\Delta_c/g^2 + 2\pi/\widetilde{\Omega},$$

should be much shorter than (i) the energy relaxation time γ_2^{-1} of the level $|2\rangle$ (note that the level $|3\rangle$ is unpopulated during the entire operation), and (ii) the lifetime of the cavity mode $\kappa^{-1} = Q/2\pi\nu_c$, where Q is the (loaded) quality factor of the cavity. These requirements can, in principle, be realized since one can (i) reduce τ by increasing the coupling constant g, (ii) increase κ^{-1} by employing a high-Q cavity so that the cavity dissipation is negligible during the operation, and (iii) choose qubit systems (e.g., atoms) with long spontaneous decay time of the level $|2\rangle$ or design qubit systems (e.g., superconducting devices) so that the energy relaxation time γ_2^{-1} of the level $|2\rangle$ is sufficiently long.

For the sake of definitiveness, let us consider the experimental possibility of realizing a six-qubit CP gate in a quantum Fourier transform (Fig. 9), using six identical superconducting qubit systems coupled to a resonator [Fig. 8(a)]. Each qubit system could be a superconducting charge-qubit system [Fig. 8(b)], flux-biased phase-qubit system [Fig. 8(c)], or flux-qubit system [Fig. 8(c)]. For the present case, qubit system 1 acts as a target instead of a control, while qubit systems (2,3,4,5,6) play the role of controls (Fig. 9). Each step of operations for implementing this gate is the same as that introduced in Sec. III. As discussed previously, to implement this gate the Rabi frequencies Ω_2, Ω_3, Ω_4, Ω_5, and Ω_6 of the pulses (respectively applied to qubit systems 2, 3, 4, 5, and 6) need to be set by $\Omega_{k+1}/\Omega_k = 1/\sqrt{2}$, leading to $\chi_{k+1}/\chi_k = 1/\sqrt{2}$ $(k = 2,3,4,5)$. By choosing $\Delta_c = 10g, \Delta' = 10\Omega_2, \Omega_2 \sim 0.9g, \widetilde{\Omega} \sim 10g$ and $m = 3$, we have (i) $\delta \sim 10g^2/\Delta_c \sim 10\Omega_2^2/\Delta' \sim 10\chi_2$, (ii) $2t_2 = \pi/\widetilde{\Omega} \sim \pi/(5g)$, and (iii) $t_3 + t_4 \sim 60\pi/g$, where $t_3 = (\pi/2)(\delta/\chi_2^2) \sim 50\pi/g$. Therefore, the condition $2t_2 \ll t_3 + t_4$ can be well satisfied. Furthermore, for the parameters chosen here, the total

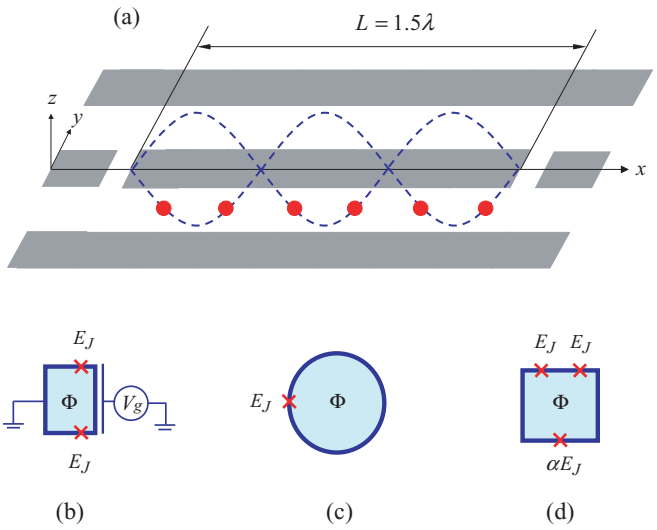

FIG. 8. (Color online) (a) Schematic diagram of the setup for six superconducting qubit systems (red dots) and a (gray) standing-wave quasione-dimensional coplanar waveguide resonator. The two blue curved lines represent the standing wave magnetic field, which is in the z direction. Each qubit system (a red dot) could be a superconducting charge-qubit system shown in (b), flux-biased phase-qubit system in (c), and flux-qubit system in (d). The qubit systems are placed at locations where the magnetic fields are the same to obtain an identical coupling constant g for each qubit system. The superconducting loop of each qubit system, which is a large square for (b) and (d) while a large circle for (c), is located in the plane of the resonator between the two lateral ground planes (i.e., the x-y plane). The external magnetic flux Φ applied to the superconducting loop for each qubit system is created by the magnetic field threading the superconducting loop; E_J is the Josephson junction energy ($0.6 < \alpha < 0.8$) and V_g is the gate voltage; λ is the wavelength of the resonator mode, and L is the length of the resonator.

operation time required for the gate implementation would be $\tau \sim 70\pi/g$.

As a rough estimate, assume $g/2\pi \sim 220$ MHz, which could be reached for a superconducting qubit system coupled to a one-dimensional standing-wave coplanar waveguide

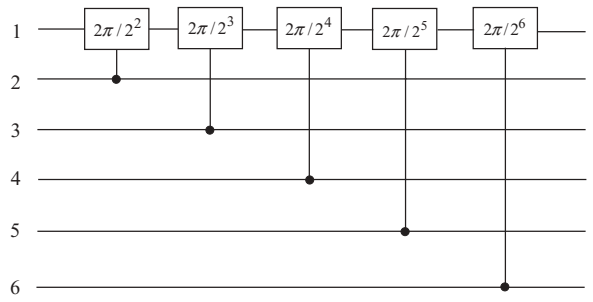

FIG. 9. Circuit for a six-qubit CP gate for the quantum Fourier transform. Here, qubits 2, 3, 4, 5, and 6 (on the filled circles) play the role of controls acting simultaneously on the target qubit 1. The element $2\pi/2^k$ represents a CP shift $\exp(i2\pi/2^k)$, which is performed on the target qubit 1 when the control qubit k is in the state $|1\rangle$ ($k = 2,3,4,5,6$). Namely, if the control qubit k is in the state $|1\rangle$, then a phase shift $2\pi/2^k$ happens to the state $|1\rangle$ of the target qubit 1, while nothing happens otherwise.

(CPW) transmission resonator [53]. For the g chosen here, we have $\tau \sim 0.16$ μs, much shorter than $\gamma_2^{-1} \sim 1$ μs [2,10]. In addition, consider a resonator with frequency $\nu_c \sim 3$ GHz (e.g., [24]) and $Q \sim 10^5$, we have $\kappa^{-1} \sim 5.3$ μs, which is much longer than the operation time τ here. Note that superconducting CPW resonators with a quality factor $Q > 10^6$ have been experimentally demonstrated [54].

How well this gate would work needs to be further investigated for each particular experimental setup or implementation. However, we note that this requires a rather lengthy and complex analysis, which is beyond the scope of this theoretical work.

VI. COMPARISON WITH PREVIOUS WORK

Several points related to this work need to be addressed. First, the present work deals with the realization of multiqubit phase gates for which the phase shifts on each target qubit are *tunable,* as shown previously. Therefore, it is much more general than our previous work [55]. Note that in [55], a method was proposed for the realization of a multiqubit phase gate which induces a *fixed* phase-shift of π on each target qubit when the control qubit is in the state $|1\rangle$. The main advantage for the method in [55] is that the cavity mode can be initially in an *arbitrary* state and thus no preparation of the initial state for the cavity mode is required. Second [56], showed how multi-ion Greenberger-Horne-Zeilinger (GHZ) entangled states can be realized based on performing a multiqubit CNOT gate with one qubit simultaneously controlling n target qubits. Since their scheme works for a special case (i.e., a CNOT on each target qubit or a *fixed* phase shift π on each target), it fails in performing other types of multiqubit phase gates for which the phase shift on each target qubit is not π. Third, we note that using the method presented in [56], a multiqubit CNOT gate or phase gate with a phase shift π on each target qubit (i.e., the first type of multiqubit gate discussed earlier) is rather difficult to implement in the other systems due to different physical mechanisms. Last, the present proposal for realizing the n successive two-qubit CP gates in QFT is different from the previous work reported in [57]. As shown previously, using the present proposal, the n successive two-qubit CP gates in QFT can be simultaneously performed using *one* single-mode cavity only. However, as argued in [57], when using the proposal in [57] to implement n successive two-qubit CP gates in QFT, n single-mode cavities would be required or a single cavity with various modes interacting qubit systems (e.g., atoms) needs to be designed.

VII. CONCLUSION

We have presented a method to realize a multiqubit *tunable* phase gate with one qubit simultaneously controlling n target qubits in a cavity QED. As shown previously, the method has the following features: (i) Neither adjustment of the level spacings of qubit systems nor adjustment of the cavity mode frequency during the gate operation is needed, thus the operation is much simplified; (ii) The operation time required for the gate realization is independent of the number of qubits and thus does not increase with the number of qubits; (iii) The n two-qubit CP gates involved can be simultaneously performed,

which significantly reduces the gate operation especially when the number n of qubits is large; (iv) The phase shift on the state of each target qubit can be *adjusted* by changing the Rabi frequencies of the pulses applied to the target qubit systems; and (v) Certain types of significant quantum CP gates with one qubit simultaneously controlling multiple target qubits or quantum CP gates with multiple control qubits simultaneously acting on one target qubit (e.g., the multiqubit phase gate in the QFT discussed previously) can be performed by using this proposal.

ACKNOWLEDGMENTS

C.P.Y. thanks Yu-xi Liu for very useful comments and is also grateful to Sahel Ashhab, Hou Ian, and Jie-Qiao Liao for their help in this work. We acknowledge partial support from the Laboratory of Physical Sciences, National Security Agency, Army Research Office, Defense Advanced Research Projects Agency, Air Force Office of Scientific Research, National Science Foundation Under Grant No. 0726909, DARPA, JSPS-RFBR under Grant No. 09-02-92114, Grant-in-Aid for Scientific Research (S), MEXT Kakenhi on Quantum Cybernetics, and FIRST (Funding Program for Innovative R&D on S&T). S. B. Zheng acknowledges support from the National Natural Science Foundation of China under Grant No. 10674025, the Doctoral Foundation of the Ministry of Education of China under Grant No. 20070386002, and funds from the State Key Laboratory Breeding Base of Photocatalysis, Fuzhou University. C. P. Yang also acknowledges funding support from the National Natural Science Foundation of China under Grant No. 11074062, the Zhejiang Natural Science Foundation under Grant No. Y6100098, the funds from Hangzhou Normal University, and the Open Fund from the SKLPS of ECNU.

APPENDIX: HOW TO HAVE THE LEVEL $|0\rangle$ NOT TO BE AFFECTED DURING THE OPERATION

As shown previously, three types of interaction are needed for the gate implementation, which are the system-cavity-pulse resonant Raman coupling, the system-cavity-pulse off-resonant Raman coupling, and the system-pulse resonant interaction. For the last type of interaction, since a resonant pulse is applied, the level $|0\rangle$ can be easily made not to be affected by the pulse, by prior adjustment of level spacings such that the transition between the level $|0\rangle$ and any one of other levels is largely detuned (decoupled) from the pulse. In the following, we will focus on how to have the level $|0\rangle$ not to be affected by the pulse and the cavity mode, for the case when the pulse is off resonant with the $|1\rangle \leftrightarrow |3\rangle$ transition and the cavity mode is off resonant with the $|2\rangle \leftrightarrow |3\rangle$ transition (i.e., the case which applies to the former two types of interactions).

To begin with, we define $\Delta_1 = |(E_1 - E_0)/\hbar - \omega|$, $\Delta_2 = |(E_2 - E_0)/\hbar - \omega|$, and $\Delta_3 = |(E_3 - E_0)/\hbar - \omega|$ as the large detuning of the pulse with the $|0\rangle \leftrightarrow |1\rangle$ transition, the large detuning of the pulse with the $|0\rangle \leftrightarrow |2\rangle$ transition, and the large detuning between the pulse and the $|0\rangle \leftrightarrow |3\rangle$ transition, respectively (Fig. 10). Here, ω is the pulse frequency. In addition, we define $\Delta_c^1 = |(E_1 - E_0)/\hbar - \omega_c|$ and $\Delta_c^2 = |(E_2 - E_1)/\hbar - \omega_c|$ as the large detuning of the cavity mode with the $|0\rangle \leftrightarrow |1\rangle$ transition and the large detuning of the cavity mode with the $|1\rangle \leftrightarrow |2\rangle$ transition, respectively (Fig. 10).

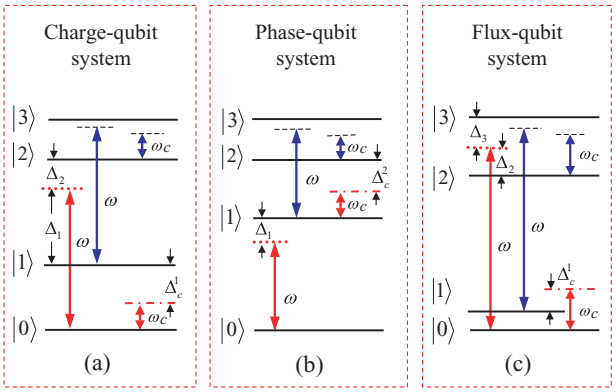

FIG. 10. (Color online) Large detuning of the pulse or the cavity mode with the transition between the level $|0\rangle$ and any one of other levels.

1. Charge-qubit system

A charge-qubit system has the level structure depicted in Fig. 3(a) [or Fig. 10(a)]. From Fig. 10(a), one can see that the dotted line falls within the range between the levels $|1\rangle$ and $|2\rangle$ in the case when the pulse is off resonant with the $|1\rangle \leftrightarrow |3\rangle$ transition. This is because the level spacing $E_2 - E_0$ is larger than the level spacing $E_3 - E_1$, resulting from $E_3 - E_2 < E_1 - E_0$ as mentioned earlier [see the caption of Fig. 3(a)]. Figure 10(a) also shows that the dot-dashed line falls within the range between the levels $|0\rangle$ and $|1\rangle$ in the case when the cavity mode is off resonant with the $|1\rangle \leftrightarrow |3\rangle$ transition. This is due to $E_3 - E_2 < E_1 - E_0$. To have the level $|0\rangle$ not to be affected by the pulse and the cavity mode, one will need to adjust the level spacings of the qubit system before the gate operation to achieve (i) the large detunings Δ_1 and Δ_2 [Fig. 10(a)], such that neither $|0\rangle \leftrightarrow |1\rangle$ transition nor $|0\rangle \leftrightarrow |2\rangle$ transition is induced by the pulse; and (ii) the large detuning Δ_c^1 [Fig. 10(a)] such that the cavity mode does not cause the $|0\rangle \leftrightarrow |1\rangle$ transition. From Fig. 10(a), it can be seen that the large detuning regime for the pulse and the $|0\rangle \leftrightarrow |3\rangle$ transition is automatically satisfied, and the large detuning of the cavity mode with the $|0\rangle \leftrightarrow |2\rangle$ or $|0\rangle \leftrightarrow |3\rangle$ transition is also automatically met. Therefore, by prior adjustment of the level spacings to have the large detunings Δ_1, Δ_2, and Δ_c^1, the level $|0\rangle$ will not be affected by the pulse and the cavity mode during the operation.

2. Phase-qubit system

A phase-qubit system has the level structure shown in Fig. 3(b) [or Fig. 10(b)]. It can be seen from Fig. 10(b) that when the pulse is off resonant with the $|1\rangle \leftrightarrow |3\rangle$ transition, the dotted line falls within the range between the two lowest levels $|0\rangle$ and $|1\rangle$, which could be achieved by adjusting the level spacings of the qubit system. In addition, Fig. 10(b) shows that the dot-dashed line falls within the range between the levels $|1\rangle$ and $|2\rangle$, in the case when the cavity mode is off resonant with the transition between the upper two levels $|2\rangle$ and $|3\rangle$. This is because of $E_2 - E_1 > E_3 - E_2$ [see the

caption of Fig. 3(b)]. To have the level $|0\rangle$ not to be affected by the pulse and the cavity mode, one will need to adjust the level spacings of the qubit system before the gate operation to obtain (i) the large detuning Δ_1 [Fig. 10(b)] such that the $|0\rangle \leftrightarrow |1\rangle$ transition induced by the pulse is avoided; and (ii) the large detuning Δ_c^2 which ensures the large detuning between the cavity mode and the $|0\rangle \leftrightarrow |1\rangle$ transition due to $E_1 - E_0 > E_2 - E_1$ [Fig. 10(b)]. In addition, Fig. 10(b) shows that the large detuning regime for the pulse and the $|0\rangle \leftrightarrow |2\rangle$ or $|0\rangle \leftrightarrow |3\rangle$ transition is automatically met, and the large detuning of the cavity mode with the $|0\rangle \leftrightarrow |2\rangle$ or $|0\rangle \leftrightarrow |3\rangle$ transition is automatically satisfied. Thus, as long as the large detunings Δ_1 and Δ_c^2 are met by prior adjustment of the level spacings, the level $|0\rangle$ will not be affected by the pulse and the cavity mode during the operation.

3. Flux-qubit system

A flux-qubit system has the level structure in Fig. 3(c) [or Fig. 10(c)]. Figure 10(c) shows that the dotted line falls within the range between the levels $|2\rangle$ and $|3\rangle$ in the case when the pulse is off resonant with the $|1\rangle \leftrightarrow |3\rangle$ transition. This is because the level spacing $E_2 - E_0$ is smaller than the level spacing $E_3 - E_1$ due to $E_1 - E_0 < E_3 - E_2$ [see the caption of Fig. 3(c)]. Figure 10(c) also shows that the dot-dashed line is above the level $|1\rangle$, which could be reached by adjusting the level spacings of the qubit system. To have the level $|0\rangle$ not to be affected by the pulse and the cavity mode, one will need to adjust the level spacings of the qubit system to achieve (i) the large detunings Δ_2 and Δ_3 [Fig. 10(c)], such that neither $|0\rangle \leftrightarrow |2\rangle$ transition nor $|0\rangle \leftrightarrow |3\rangle$ transition is induced by the pulse; and (ii) the large detuning Δ_c^1 [Fig. 10(c)], to avoid the $|0\rangle \leftrightarrow |1\rangle$ transition induced by the cavity mode. From Fig. 10(c), it can be seen that the large detuning regime for the pulse and the $|0\rangle \leftrightarrow |1\rangle$ transition is automatically satisfied, and the large detuning of the cavity mode with the $|0\rangle \leftrightarrow |2\rangle$ or $|0\rangle \leftrightarrow |3\rangle$ transition is automatically met. Hence, as long as the large detunings Δ_2, Δ_3, and Δ_c^1 are satisfied by prior adjustment of the level spacings, the level $|0\rangle$ will not be affected during the operation. We here should mention that because the dotted line falls within the range between the upper two levels $|2\rangle$ and $|3\rangle$ [Fig. 10(c)], a more careful adjustment of the level spacings would be needed to obtain the large detunings Δ_1 and Δ_2 for the flux-qubit system, when compared with the charge-qubit system or the phase-qubit system.

[1] J. Q. You and F. Nori, Phys. Today **58**, 42 (2005).
[2] J. Clarke and F. K. Wilhelm, Nature (London) **453**, 1031 (2008).
[3] I. Buluta and F. Nori, Science **326**, 108 (2009).
[4] T. D. Ladd, F. Jelezko, R. Laflamme, Y. Nakamura, C. Monroe, and J. L. OBrien, Nature (London) **464**, 45 (2010).
[5] A. Blais, J. Gambetta, A. Wallraff, D. I. Schuster, S. M. Girvin, M. H. Devoret, and R. J. Schoelkopf, Phys. Rev. A **75**, 032329 (2007).
[6] M. A. Sillanpää, J. I. Park, and R. W. Simmonds, Nature (London) **449**, 438 (2007).
[7] R. J. Schoelkopf and S. M. Girvin, Nature (London) **451**, 664 (2008).
[8] M. Hofheinz, E. M. Weig, M. Ansmann, R. C. Bialczak, E. Lucero, M. Neeley, A. D. OConnell, H. Wang, J. M. Martinis, and A. N. Cleland, Nature (London) **454**, 310 (2008).
[9] M. Hofheinz *et al.*, Nature (London) **459**, 546 (2009).
[10] L. DiCarlo *et al.*, Nature (London) **460**, 240 (2009).
[11] J. Q. You and F. Nori, Phys. Rev. B **68**, 064509 (2003).
[12] J. Q. You, J. S. Tsai, and F. Nori, Phys. Rev. B **68**, 024510 (2003).
[13] A. Blais, R. S. Huang, A. Wallraff, S. M. Girvin, and R. J. Schoelkopf, Phys. Rev. A **69**, 062320 (2004).
[14] C. P. Yang, Shih-I. Chu, and S. Han, Phys. Rev. Lett. **92**, 117902 (2004).
[15] L. I. Childress, A. S. Sorensen, and M. D. Lukin, Phys. Rev. A **69**, 042302 (2004).
[16] A. Wallraff, D. I. Schuster, A. Blais, L. Frunzio, R.-S. Huang, J. Majer, S. Kumar, S. M. Girvin, and R. J. Schoelkopf, Nature (London) **431**, 162 (2004).
[17] I. Chiorescu, P. Bertet, K. Semba, Y. Nakamura, C. J. P. M. Harmans, and J. E. Mooij, Nature (London) **431**, 159 (2004).
[18] G. Khitrova, H. M. Gibbs, M. Kira, S. W. Koch, and A. Scherer, Nat. Phys. **2**, 81 (2006).
[19] Q. A. Turchette, C. J. Hood, W. Lange, H. Mabuchi, and H. J. Kimble, Phys. Rev. Lett. **75**, 4710 (1995).
[20] A. Rauschenbeutel, G. Nogues, S. Osnaghi, P. Bertet, M. Brune, J. M. Raimond, and S. Haroche, Phys. Rev. Lett. **83**, 5166 (1999).
[21] J. A. Jones, M. Mosca, and R. H. Hansen, Nature (London) **393**, 344 (1998).
[22] J. H. Plantenberg, P. C. de Groot, C. J. P. M. Harmans, and J. E. Mooij, Nature (London) **447**, 836 (2007).
[23] J. Majer *et al.*, Nature (London) **449**, 443 (2007).
[24] P. J. Leek, S. Filipp, P. Maurer, M. Baur, R. Bianchetti, J. M. Fink, M. Göppl, L. Steffen, and A. Wallraff, Phys. Rev. B **79**, 180511(R) (2009).
[25] R. C. Bialczak *et al.*, Nat. Phys. **6**, 409 (2010).
[26] A. Barenco, C. H. Bennett, R. Cleve, D. P. DiVincenzo, N. Margolus, P. Shor, T. Sleator, J. A. Smolin, and H. Weinfurter, Phys. Rev. A **52**, 3457 (1995).
[27] M. Möttönen, J. J. Vartiainen, V. Bergholm, and M. M. Salomaa, Phys. Rev. Lett. **93**, 130502 (2004).
[28] T. Monz, K. Kim, W. Hänsel, M. Riebe, A. S. Villar, P. Schindler, M. Chwalla, M. Hennrich, and R. Blatt, Phys. Rev. Lett. **102**, 040501 (2009).
[29] X. Wang, A. Sørensen, and K. Mølmer, Phys. Rev. Lett. **86**, 3907 (2001).
[30] L.-M. Duan, B. Wang, and H. J. Kimble, Phys. Rev. A **72**, 032333 (2005).
[31] C. P. Yang and S. Han, Phys. Rev. A **72**, 032311 (2005); **73**, 032317 (2006).
[32] X.-M. Lin, Z. W. Zhou, M. Y. Ye, Y. F. Xiao, and G. C. Guo, Phys. Rev. A **73**, 012323 (2006).
[33] S. B. Zheng and G. C. Guo, Phys. Rev. A **73**, 052328 (2006).
[34] G. W. Lin, X. B. Zou, M. Y. Ye, X. M. Lin, and G. C. Guo, Phys. Rev. A **77**, 032308 (2008).

[35] M. Neeley, M. Ansmann, R. C. Bialczak, M. Hofheinz, N. Katz, E. Lucero, A. O'Connell, H. Wang, A. N. Cleland, and J. M. Martinis, Nat. Phys. **4**, 523 (2008); A. M. Zagoskin, S. Ashhab, J. R. Johansson, and F. Nori, Phys. Rev. Lett. **97**, 077001 (2006).

[36] Y. X. Liu, J. Q. You, L. F. Wei, C. P. Sun, and F. Nori, Phys. Rev. Lett. **95**, 087001 (2005).

[37] M. Brune, E. Hagley, J. Dreyer, X. Maitre, A. Maali, C. Wunderlich, J. M. Raimond, and S. Haroche, Phys. Rev. Lett. **77**, 4887 (1996).

[38] M. Sandberg, C. M. Wilson, F. Persson, T. Bauch, G. Johansson, V. Shumeiko, T. Duty, and P. Delsing, Appl. Phys. Lett. **92**, 203501 (2008).

[39] A. Palacios-Laloy, F. Nguyen, F. Mallet, P. Bertet, D. Vion, and D. Esteve, J. Low Temp. Phys. **151**, 1034 (2008).

[40] J. R. Johansson, G. Johansson, C. M. Wilson, and F. Nori, Phys. Rev. Lett. **103**, 147003 (2009).

[41] J. Q. Liao, Z. R. Gong, L. Zhou, Y. X. Liu, C. P. Sun, and F. Nori, Phys. Rev. A **81**, 042304 (2010).

[42] L. Wang, R. R. Puri, and J. H. Eberly, Phys. Rev. A **46**, 7192 (1992).

[43] C. P. Yang, Shih-I. Chu, and S. Han, Phys. Rev. A **70**, 044303 (2004); J. Phys.: Condensed Matter **16**, 1907 (2004).

[44] S. B. Zheng and G. C. Guo, Phys. Rev. Lett. **85**, 2392 (2000); S. B. Zheng, *ibid.* **87**, 230404 (2001).

[45] A. Sørensen and K. Mølmer, Phys. Rev. Lett. **82**, 1971 (1999).

[46] For atoms, the level spacings can be changed via adjusting the external electronic field. For the details see P. Pradhan, M. P. Anantram, and K. L. Wang, e-print arXiv:quant-ph/0002006.

[47] M. Šašura and V. Buzek, Phys. Rev. A **64**, 012305 (2001).

[48] F. Gaitan, *Quantum Error Correction and Fault Tolerant Quantum Computing* (CRC Press, Boca Raton, FL, 2008).

[49] T. Beth and M. Rötteler, *Quantum Information* (Springer, Berlin, 2001), Vol. 173, Ch. 4, p. 96.

[50] S. L. Braunstein, V. Buzek, and M. Hillery, Phys. Rev. A **63**, 052313 (2001).

[51] P. W. Shor, in *Proceedings of the 35th Annual Symposium on Foundations of Computer Science*, edited by S. Goldwasser (IEEE Computer Society Press, Los Alamitos, CA, 1994), Vol. 124.

[52] M. A. Nielsen and I. L. Chuang, *Quantum Computation and Quantum Information* (Cambridge University Press, Cambridge, England, 2001).

[53] L. DiCarlo, M. D. Reed, L. Sun, B. R. Johnson, J. M. Chow, J. M. Gambetta, L. Frunzio, S. M. Girvin, M. H. Devoret, and R. J. Schoelkopf, Nature (London) **467**, 574 (2010).

[54] P. K. Day, H. G. LeDuc, B. A. Mazin, A. Vayonakis, and J. Zmuidzinas, Nature (London) **425**, 817 (2003).

[55] C. P. Yang, Y. X. Liu, and F. Nori, Phys. Rev. A **81**, 062323 (2010).

[56] J. Steinbach and C. C. Gerry, Phys. Rev. Lett. **81**, 5528 (1998).

[57] M. O. Scully and M. S. Zubairy, Phys. Rev. A **65**, 052324 (2002).